

Hall effect measurements using low ac magnetic fields and lock-in technique on field effect transistors with molybdenum disulfide channels

Yoshihiro Shimazu*, Tatsuya Iwabuchi, Kensuke Arai, Inoru Shioya

Department of Physics, Yokohama National University, Hodogaya 79-5, Yokohama 240-8501, Japan

*E-mail: yshimazu@ynu.ac.jp

Keywords: Hall effect, molybdenum disulfide, transition-metal dichalcogenide, two-dimensional material, carrier density, field effect transistor

ABSTRACT

Hall effect measurements conventionally rely on the use of dc magnetic fields. For electronic devices made of ultrathin semiconducting materials, such as molybdenum disulfide (MoS_2), the dc Hall effect measurements have practical difficulties. Here, we report the results of the Hall effect measurements using ac magnetic fields and a lock-in detection of the Hall voltage for field effect transistors with ultrathin MoS_2 channels. The ac Hall effect measurements have some advantages over the dc measurements. The carrier concentration and the Hall mobility were estimated as a function of gate voltage from the results of the ac Hall effect measurements. They used a magnetic field strength that was lower by two orders of magnitude than those used in prior studies on MoS_2 devices, which relied on dc magnetic fields.

1. Introduction

Molybdenum disulfide (MoS_2), a prototypical semiconducting transition-metal dichalcogenide, has attracted a lot of interest as one of the promising materials for nanoelectronic and nano-optoelectronic devices [1-6]. In particular, field effect transistors (FETs) that use MoS_2 as a channel material have been studied intensively. High electron mobilities have been reported for monolayer MoS_2 FETs [7]. In the study of MoS_2 devices and similar two-dimensional materials, it is crucial to measure the basic material parameters, such as carrier concentration and carrier mobility. Conventionally, the carrier concentration is estimated on the basis of the results of the Hall effect measurement. However, the Hall effect measurement on FETs with atomically thin MoS_2 channels has associated practical difficulties; the results of Hall effect measurements of MoS_2 FETs have been reported only in a limited number of papers [8-12]. The difficulties in this measurement include (1) the severely limited bias current allowed for atomically thin devices, (2) the high voltage noise associated with a large amount of localized states [13], and (3) a high contact resistance owing to the Schottky barrier at the contact junction [14-21]. The localized states are associated with carrier trapping–detrapping process, which may contribute to fluctuations in carrier mobility or carrier number [22,23], manifesting as voltage noise. It is noteworthy that the past Hall effect measurements of the MoS_2 FETs were demonstrated for devices with relatively high carrier densities that were induced by top-gating with a thin dielectric [8] or by ionic-liquid gating [9], and for devices with relatively low contact resistance achieved by vacuum annealing leading to a nearly complete elimination of the Schottky barrier

[11], or by graphene contacts [12].

The Hall voltage is given by

$$V_H = \frac{R_H IB}{t}$$

where R_H , I , B , and t are the Hall coefficient, flowing bias current, magnetic field, and film thickness, respectively [24,25]. The Hall coefficient is related to the carrier concentration n , by the relation

$$R_H = -\frac{1}{ne},$$

where e is the electronic charge. Here, we assume that the Hall scattering factor, $r = 1$ [24,25], where r is given by $r = \langle \tau^2 \rangle / \langle \tau \rangle^2$, where τ is the mean time between carrier collisions [26]. For devices made of two-dimensional materials such as MoS₂, with thicknesses less than ~ 100 nm, the bias current that can flow without destroying the devices is severely limited, typically to less than $100 \mu\text{A}$. In prior studies on MoS₂ devices [8-12], it was common in Hall effect measurements to apply dc magnetic fields with magnitudes of several Teslas to measure the Hall voltage. The observed Hall voltage measured using even such high magnetic fields is noisy, as has been reported in the past literature [8], which may lead to an inaccurate estimate of the Hall voltage, and, in turn, the carrier concentration.

In contrast to dc magnetic fields that are commonly applied, we, in this work, used ac magnetic fields and measured the Hall voltage by a lock-in technique. This method should allow the measurement of a very small Hall voltage in a noisy environment. We can measure the intrinsic Hall voltage by a lock-in technique by modulating either the magnetic field or bias current in an ideal case. However, in reality, the lock-in detection of a small V_H using an ac bias current, rather than an ac magnetic field, is very difficult. This is because the misalignment of the Hall voltage probes, which always exists in actual samples, induces a considerable transverse voltage that overwhelms the intrinsic V_H . Therefore, the measured transverse voltage, which should be equal to V_H without the misalignment, is expressed as

$$V_m = IR_S(\mu B + \alpha) + V_0,$$

where R_S , μ , α , and V_0 are the sheet resistance, mobility, a geometrical factor quantifying the misalignment of the Hall voltage probes, and a constant offset voltage, respectively [25]. When the bias current is modulated with an amplitude I , the amplitude of V_m measured by the lock-in technique at a constant magnetic field B is

$$V_m^*(B) = \frac{1}{2}(V_m(I, B) - V_m(-I, B)) = IR_S(\mu B + \alpha).$$

In typical measurements of MoS₂ FETs, the spurious voltage due to the misalignment is considerably larger than the intrinsic Hall voltage, that is, $IR_S\mu B \ll IR_S\alpha$. The ratio of $IR_S\alpha$ to $IR_S\mu B$ was typically greater than 100 in our measurements. Therefore, measuring the intrinsic Hall voltage by modulating the bias current is impractical.

In contrast, if we modulate the magnetic field with an amplitude B , the measured amplitude of V_m at constant I is given by

$$V_m^*(I) = \frac{1}{2}(V_m(I, B) - V_m(I, -B)) = IR_S\mu B.$$

This implies that the intrinsic Hall voltage can be detected using the lock-in technique by modulating the applied magnetic field. In actual measurement apparatuses, even ac magnetic fields can generally be associated with spurious oscillations of V_m , owing to the spurious coupling of the magnetic fields, which may partly originate from electromagnetic induction. In this case, the measured amplitude of V_m using ac magnetic fields is given by

$$V_m^*(I) = \frac{1}{2}(V_m(I, B) - V_m(I, -B)) = IR_S\mu B + cB. \quad (c \text{ is a constant}).$$

Here, cB is the amplitude of the spurious oscillating component that is in phase with magnetic field oscillations. In our measurements of Hall voltage, described later, the second term cB was of the same order of magnitude as $IR_S\mu B$. We can determine the intrinsic Hall voltage by measuring V_m for the currents in opposite directions. The intrinsic Hall voltage ($V_H = IR_S\mu B$) is obtained from the equation

$$V_H = \frac{1}{2}(V_m^*(I) - V_m^*(-I)),$$

where $V_m^*(I)$ and $V_m^*(-I)$ are the measured oscillation amplitudes of V_m for dc bias currents in opposite directions.

In this paper, we present the results of the Hall effect measurements on a MoS₂ FET using ac magnetic fields and a lock-in technique. The carrier concentration and the Hall mobility were successfully estimated as a function of the gate voltage, using low ac magnetic fields, which is lower by two orders of magnitude than the magnetic fields that were commonly applied in prior dc Hall effect measurements on MoS₂ devices.

2. Frequency characteristics of the ac Hall-effect measurement system

To find the optimum frequency for magnetic field modulation, we examined the frequency characteristics of our measurement apparatus. First, the frequency response of the lock-in amplifier (EG&G 5210) was measured according to the schematic shown in Fig. 1(a). A sinusoidal signal with an amplitude V_{in} produced by a function generator was fed into the lock-in amplifier. Because the frequency range of the lock-in amplifier was limited to the range of 0.5 Hz to 120 kHz, the amplitude, V_{meas} , recorded by the lock-in amplifier was significantly less than that of the input signal at very low and high frequencies. As shown in Fig. 2, the measured ratio V_{meas}/V_{in} decreased rapidly with decreasing frequency, with a cut-off frequency of ~ 0.6 Hz.

Second, we examined the frequency response of the magnet used in our measurement in terms of the ratio B_0/I_0 , where B_0 and I_0 are the amplitude of the ac magnetic field and that of the ac magnet current that flowed through the magnet. The method for measuring B_0/I_0 is schematically shown in Fig. 1(b). We used a large iron-core magnet (Oki Electric Industry, dc 60 A, 2 T) to apply the magnetic field. An ac magnet current was applied using a function generator and homemade power amplifier. The magnetic field produced by the magnet was detected by a Hall sensor (Toshiba THS126). We measured the amplitude of

the ac Hall voltage of the Hall sensor by using a differential amplifier and an oscilloscope. The ratio B_0/I_0 obtained in this measurement is shown in Fig. 2. Note that B_0/I_0 shown in this figure was normalized so that the value became unity as the frequency tended to zero. B_0/I_0 decreased rapidly with increasing frequency, owing to the slow response of the magnet. The oscillations of B_0 and I_0 were not in phase because of the hysteretic response of the magnet.

In our ac Hall effect measurement on MoS₂ devices, we measured a very small oscillation amplitude of the Hall voltage using the lock-in amplifier with very high sensitivity. Owing to the limitation in the amount of dissipated power in the power amplifier for generating magnet current, the allowable amplitude of the applied ac magnet current was limited, almost irrespective of the used frequency. Therefore, the overall frequency response of our ac Hall-effect measurement system is given by the product of the two characteristics ($V_{\text{meas}}/V_{\text{in}}$ and B_0/I_0) shown in Fig. 2. The overall frequency response obtained, which is denoted as V_{meas}/I_0 (normalized), has a peak as shown in Fig. 3. The frequencies for the maximum response are in the range of 0.5–0.9 Hz. To reduce the time required for the lock-in measurement, the optimum frequency was estimated as ~0.9 Hz.

3. Experimental results of MoS₂ FET

We fabricated MoS₂ devices with a back-gated field effect transistor geometry. Figure 4 shows the optical image of the device. The MoS₂ flake (~15 nm thickness) was exfoliated from bulk MoS₂ (SPI supplies) and deposited on a Si substrate covered with 270-nm SiO₂. The exfoliation was performed using an adhesive tape and a gel sheet [27,28]. The highly doped Si substrate was used as a back gate. The contact electrodes (Ti 15 nm/Au 75 nm) were patterned by photolithography and deposited using e-beam evaporation. The four-terminal conductance and the Hall voltage were measured for various values of drain-to-source voltage, V_{ds} , and the back-gate voltage, V_{g} , in air at room temperature (290 K).

Figure 5 shows the four-terminal sheet conductance G_{s} as a function of V_{g} , which indicates the characteristics of the N-channel FET. The $G_{\text{s}}-V_{\text{g}}$ curve is linearly fitted as shown by the dashed line in Fig. 5. The field effect mobility can be derived from the slope of the $G_{\text{s}}-V_{\text{g}}$ curve in the linear regime, using the expression

$$\mu_{\text{FE}} = \frac{dG_{\text{s}}}{dV_{\text{g}}} \cdot \frac{1}{C_{\text{i}}},$$

where $C_{\text{i}} = 13 \text{ nF/cm}^2$ is the capacitance between the channel and the back gate per unit area [7]. The mobility thus determined is $6.5 \text{ cm}^2 \text{ V}^{-1} \text{ s}^{-1}$. This value is lower than those reported previously for back-gated MoS₂ FETs; for example, $\sim 15 \text{ cm}^2 \text{ V}^{-1} \text{ s}^{-1}$ was reported for monolayer [8] and multilayer back-gated MoS₂ FETs [29] on SiO₂ dielectric. The contact resistances of the source and drain electrodes can be estimated by subtracting the channel resistance from the total (two-terminal) resistance [30]. The channel resistance is estimated using G_{s} and the channel length/width between the electrodes. Thus, the contact resistances at $V_{\text{g}} = 50 \text{ V}$ are found to be $\sim 800 \text{ k}\Omega \mu\text{m}$. This value is considerably higher than the contact resistances $\sim 2 \text{ k}\Omega \mu\text{m}$ reported for Mo contact and optimal Ti contact [30].

We carried out ac Hall effect measurements on this device. The frequency and amplitude of the ac

magnetic fields were 0.9 Hz and 0.024 T, respectively. The time trace of the oscillation amplitudes (V_m^*) of the transverse voltage for currents in opposite directions were measured by the lock-in amplifier, as shown in Fig. 6. For each value of V_{ds} (2.5 V and -2.5 V), we recorded time traces of V_m^* and drain-to-source current I_{ds} , and derived the time averages of V_m^* and I_{ds} from these. The time traces for the total time of 960 s were used to calculate the time averages for each value of V_{ds} . The uncertainty of the time averages were estimated as the standard error, which was the standard deviation of the time traces divided by \sqrt{N} , where we assumed $N = 960 \text{ s} / (3\tau)$ and $\tau = 30 \text{ s}$ (time constant of the lock-in amplifier). The above procedure was repeated for different values of V_g from -40 to 50 V . Figure 7 shows the transverse resistance R_{xy} as a function of B (amplitude of ac magnetic fields) at $V_g = 50 \text{ V}$, where

$$R_{xy} = \frac{1}{2I} (V_m^*(I) - V_m^*(-I)).$$

Based on the equation given in Section 1, $R_{xy} = V_H / I = R_S \mu B = \frac{R_H B}{t}$; therefore, R_{xy} should be proportional to B . The expected linear relationship between R_{xy} and B is indicated by the data shown in Fig. 7.

The sheet electron density, n , derived from the ratio R_{xy}/B , is shown as a function of V_g , in Fig. 8. The highest n observed in this measurement was $2.7 \times 10^{12} \text{ cm}^{-2}$, at $V_g = 50 \text{ V}$. Under the approximation that the gate capacitance is that of a parallel-plate capacitor with a 270-nm SiO_2 dielectric, the derivative of the sheet electron density with respect to V_g is given by

$$\frac{dn}{dV_g} = \frac{C_i}{e}.$$

This value is consistent with the slope of the n - V_g curve in the higher V_g range, as shown in Fig. 8. The uncertainty of the measured n is predominantly determined by the fluctuation of V_m^* as indicated in Fig. 6. It should be noted that the uncertainty due to the statistical fluctuations decreases with an increase in the duration of the measurement. Alternatively, the fractional uncertainty of n should decrease significantly when the amplitude of the ac magnetic fields increases. This improvement should be possible by changing the magnet or power amplifier used to apply the magnet current. Besides the field strength, the optimum frequency can be increased by using a suitable magnet. At higher modulation frequency and a fixed measurement time, the fractional uncertainty ratio is expected to decrease significantly, because the standard error of the time traces would become smaller. The dominant frequencies of the fluctuations of V_m^* as shown in Fig. 6 are below $\sim 0.03 \text{ Hz}$ because the time constant of the lock-in amplifier in the measurement is 30 s. The large gradual fluctuation may be caused by noise from outside and that intrinsic to the device. The intrinsic noise can be attributed to $1/f$ current noise [31], which has been observed in MoS_2 FETs [22,23]. The origin of the $1/f$ noise is proposed to be fluctuations in carrier mobility and/or carrier number [22,23]. It has been suggested that the intrinsic noise levels could be reduced in suspended geometries or surface passivation [22].

The calculated Hall mobility $\mu_H = \frac{G_s}{ne}$ is also shown in Fig. 8. μ_H increases with increasing V_g , then

saturates at $V_g \sim 20\text{V}$. Subsequently, it decreases with an increase in V_g up to 50 V. Similar dependences of μ_H on V_g have been reported for back-gated FETs and electric double layer transistors (EDLT) with a MoS_2 channel [9,10]. The increase in μ_H with an increase in V_g is attributed to a decrease in the Coulomb scattering with an increasing carrier density [10]. The difference between μ_H and μ_{FE} can be partly attributed to dependence of the intrinsic mobility on the carrier density [11].

4. Discussion and conclusions

In conventional Hall effect measurements, dc magnetic fields are used, because magnets that produce high magnetic fields are associated with a large amount of inductance, which makes it difficult to alternate magnetic fields. In the dc Hall effect measurements, to eliminate the offset voltage due to misalignment of the Hall voltage probes, it is customary to measure the Hall voltages with the magnetic fields in opposite directions. These measurements can take a considerable amount of time because the stabilization of the magnetic fields and the Hall voltages can take as long as several minutes. For such slow measurements, the temporal variation in the sample characteristics, including resistivity, and external parameters including temperature, must be compensated to achieve a reliable estimate of the carrier concentration [25]. In ref. [25] the dc Hall effect measurement is demonstrated for low-mobility thin films (mobility values well below $1\text{cm}^2/\text{Vs}$) using the compensation methods. In comparison to the dc Hall effect measurement, the ac measurement scheme presented in this work is particularly advantageous in that the measurement time can be less than several seconds. This is because the ac modulation frequency for the magnetic fields can be chosen to be higher than 1 Hz. Therefore, the temporal variations in the sample parameters and external parameters are negligible and the compensation schemes, as presented in ref. [25], that are required for the dc Hall effect measurement are not necessary. In addition to the excellent suppression of the noise associated with the lock-in technique, the advantage of having a short measurement time may compensate for the drawback of the ac Hall effect measurement, that is, the limitation of the amplitude of the applied magnetic fields. In addition, from the view point of cost of experiment, the ac Hall effect measurement is advantageous because high magnetic fields $> 1\text{T}$ are not required. The field amplitude 0.024 T used in our measurement is lower by two orders of magnitude than those used in prior dc Hall effect measurements on MoS_2 FETs (1 T [11] and $> 9\text{T}$ [8,9,12]).

Using the ac Hall effect measurements, we successfully measured the carrier concentration and the Hall mobility in FETs with ultrathin MoS_2 channels in air at room temperature. Despite the large voltage noise that may be associated with the localized states and trapped charge, the Hall voltage was unambiguously detected by the lock-in technique. The dependences of the carrier concentration and the Hall mobility on V_g are consistent with those reported previously. The mobility is lower and the contact resistances are higher in the sample we studied in comparison to those typically reported in the past studies on MoS_2 FETs. Low mobility and high contact resistances result in difficulties in conducting Hall effect measurements. In particular, low mobility is generally associated with low Hall voltage, and four-terminal measurements are challenging for very high contact resistances. However, the field strength required for the Hall effect measurement in this work is lower by two orders of magnitude than those used in prior studies

on MoS₂ devices, which relied on dc magnetic fields. We have demonstrated the ac Hall effect measurements for multilayer MoS₂ flakes. The ac Hall effect measurement scheme presented in this paper may be applied to monolayer MoS₂ and other two-dimensional materials as well.

Acknowledgements

This work was partly supported by JSPS KAKENHI Grant Numbers 15K13497 and 19K03697.

References

- [1] Q. H. Wang, K. Kalantar-Zadeh, A. Kis, J. N. Coleman, M. S. Strano, *Nat. Nanotechnol.* **7**, 699 (2012).
- [2] X. Tong, E. Ashalley, F. Lin, H. Li, Z. M. Wang, *Nano-Micro Lett.* **7**, 203 (2015).
- [3] A. Rai, H. C. P. Movva, A. Roy, D. Taneja, S. Chowdhury, and S. K. Banerjee, *Crystals* **8**, 316 (2018).
- [4] G. R. Bhimanapati, Z. Lin, V. Meunier, Y. Jung, J. Cha, S. Das, D. Xiao, Y. Son, M. S. Strano, V. R. Cooper, L. Liang, S. G. Louie, E. Ringe, W. Zhou, S. S. Kim, R. R. Naik, B. G. Sumpter, H. Terrones, F. Xia, Y. Wang, J. Zhu, D. Akinwande, N. Alem, J. A. Schuller, R. E. Schaak, M. Terrones, J. A. Robinson, *ACS Nano* **9**, 11509 (2015).
- [5] A. Gupta, T. Sakhivel, S. Seal, *Prog. Mater. Sci.* **73**, 44. (2015).
- [6] M. Chhowalla, D. Jena, H. Zhang, *Nat. Rev. Mater.* **1**, 16052 (2016).
- [7] B. Radisavljevic, A. Radenovic, J. Brivio, V. Giacometti, A. Kis, *Nat. Nanotechnol.* **6**, 147 (2011).
- [8] B. Radisavljevic, A. Kis, *Nat. Mater.* **12**, 815 (2013).
- [9] Y. Zhang, J. Ye, Y. Matsushashi, Y. Iwasa, *Nano Lett.* **12**, 1136 (2012).
- [10] A. T. Neal, H. Liu, M. Si, Y. Deng, J. Gu, P. D. Ye, *ACS Nano* **7**, 7077 (2013).
- [11] B. W. H. Baugher, H. O. H. Churchill, Y. Yang, P. Jarillo-Herrero, *Nano Lett.* **13**, 4212 (2013).
- [12] X. Cui, G.-H. Lee, Y. D. Kim, G. Arefe, P. Y. Huang, C.-H. Lee, D. A. Chenet, X. Zhang, L. Wang, F. Ye, F. Pizzocchero, B. S. Jessen, K. Watanabe, T. Taniguchi, D. A. Muller, T. Low, P. Kim, J. Hone, *Nat. Nanotechnol.* **10**, 534 (2015).
- [13] W. Zhu, T. Low, Y.-H. Lee, H. Wang, D. B. Farmer, J. Kong, F. Xia, P. Avouris, *Nat. Commun.* **5**:3087 (2014).
- [14] A. Allain, J. Kang, K. Banerjee, A. Kis, *Nat. Mater.* **14**, 1195 (2015).
- [15] I. Popov, G. Seifert, D. Tomanek, *Phys. Rev. Lett.* **108**, 156802 (2012).
- [16] S. McDonnell, R. Addou, C. Buie, R. M. Wallace, C. L. Hinkle, *ACS Nano* **8**, 2880 (2014).
- [17] S. Walia, S. Balendhran, Y. Wang, R. A. Kadir, A. S. Zoofakar, P. Atkin, J. Z. Ou, S. Sriram, K. Kalantar-zadeh, M. Bhaskaran, *Appl. Phys. Lett.* **103**, 232105 (2013).
- [18] H. Liu, M. Si, Y. Deng, A. T. Neal, Y. Du, S. Najmaei, P. M. Ajayan, J. Lou, P. D. Ye, *ACS Nano* **8**, 1031 (2014).
- [19] W. Liu, J. Kang, D. Sarkar, Y. Khatami, D. Jena, K. Banerjee, *Nano Lett.* **13**, 1983 (2013).

- [20] S. Das, H.-Y. Chen, A. V. Penumatcha, J. Appenzeller, Nano Lett. **13**, 100 (2013).
- [21] C. D. English, G. Shine, V. E. Dorgan, K. C. Saraswat, E. Pop, Nano Lett. **16**, 3824 (2016).
- [22] V. K. Sangwan, H. N. Arnold, D. Jariwala, T. J. Marks, L. J. Lauhon, and M. C. Hersam, Nano Lett. **13**, 4351 (2013).
- [23] I. Martinez, M. Ribeiro, P. Andres, L. E. Hueso, F. Casanova, and F. G. Aliev, Phys. Rev. Applied **7**, 034034 (2017).
- [24] S. M. Sze, *Semiconductor Devices: Physics and Technology* (Wiley, New York, 2002) 2nd ed.
- [25] F. Werner, J. Appl. Phys. **122**, 135306 (2017).
- [26] D. K. Schroder, *Semiconductor Material and Device Characterization* (Wiley, New Jersey, 2006).
- [27] K. S. Novoselov, A. K. Geim, S. V. Morozov, D. Jiang, Y. Zhang, S. V. Dubonos, I. V. Grigorieva, A. A. Firsov, Science **306**, 666 (2004).
- [28] A. Castellanos-Gomez, M. Buscema, R. Molenaar, V. Singh, L. Janssen, H. S. J. van der Zant, G. A. Steele, 2D Mater. **1**, 011002 (2014).
- [29] H.-J. Kwon, J. Jang, S. Kim, V. Subramanian, and C. P. Grigoropoulos, Appl. Phys. Lett. **105**, 152105 (2014).
- [30] J. Kang, W. Liu, and K. Banerjee, and A. Kis, Appl. Phys. Lett. **104**, 093106 (2014).
- [31] F. N. Hooge, Phys. Lett. **29A**, 139 (1969).

Figure captions

Fig. 1. Schematics of setup for measurement of frequency response of the lock-in amplifier (a) and magnet (b). Dependence of V_{meas} on V_{in} and that of B_0 on I_0 are measured, where V_{in} , B_0 , and I_0 are the oscillation amplitudes of the input signal, magnetic field, and magnet current, respectively. V_{meas} is the amplitude recorded by the lock-in amplifier. The magnetic field is measured using a Hall sensor, of which the Hall voltage is read out using the differential amplifier and oscilloscope. In the actual Hall effect measurements on MoS₂ devices, the Hall sensor is replaced with a MoS₂ flake, and the very small output signal of the differential amplifier is fed into the lock-in amplifier.

Fig. 2. Frequency characteristics of the ac Hall effect measurement system used in this work. The ratios $V_{\text{meas}}/V_{\text{in}}$ (black squares) and B_0/I_0 (blue triangles) are shown as a function of frequency, where V_{meas} , V_{in} , B_0 , and I_0 are the voltage amplitude measured by the lock-in amplifier, the amplitudes of input-voltage oscillations, magnetic field measured by a Hall sensor, and the applied ac magnet current, respectively. Here, B_0/I_0 is shown as a normalized value so that the value is unity as the frequency tends to zero.

Fig. 3. The ratio V_{meas}/I_0 as a function of frequency, which is the overall frequency characteristics of the ac Hall effect measurement system. When the amplitude of the magnet current is fixed, the measured Hall voltage is proportional to this value.

Fig. 4. Optical micrograph of the MoS₂ FET device. Scale bar is 50 μm . The dc bias current flowed between the drain and source terminals (D and S). The Hall voltage was measured using the Hall voltage probes (V_1 and V_3). The four-terminal resistance was obtained using the voltage between the voltage probes (V_1 and V_2). The channel length between the drain and source terminals and the channel width were $L = 26\mu\text{m}$ and $W = 65\mu\text{m}$, respectively.

Fig. 5. The four-terminal sheet conductance G_s of the MoS₂ FET device as a function of V_g . The field effect mobility is derived from the slope of the G_s - V_g curve in the linear regime as shown in the text.

Fig. 6. Time traces of drain-to-source voltage V_{ds} and amplitude V_m^* of the oscillation component of the transverse voltage that are in phase with magnetic field oscillations, acquired by the lock-in amplifier. The unit of time ΔT was 160 s. V_{ds} was switched between 2.5 V and -2.5 V, with a period of $4\Delta T$. For each value of V_{ds} , V_m^* was recorded for the time interval of ΔT after waiting time of ΔT , so that the device reaches an equilibrium state.

Fig. 7. Transverse resistance R_{xy} as a function of B (amplitude of ac magnetic fields) at $V_g = 50$ V. From the slope of the fitted line, the sheet electron density was estimated to be $3.7 \times 10^{12} \text{ cm}^{-2}$. This value is different from that shown in Fig. 8 ($2.7 \times 10^{12} \text{ cm}^{-2}$), because the data of Fig. 7 were measured six months after the measurement for Fig. 8.

Fig. 8. The sheet electron density n and the Hall mobility μ_{H} as a function of V_g acquired in the ac Hall effect measurements. μ_{H} is obtained from n and the four-terminal sheet resistance. The frequency of the ac magnetic fields was 0.9 Hz in this measurement.

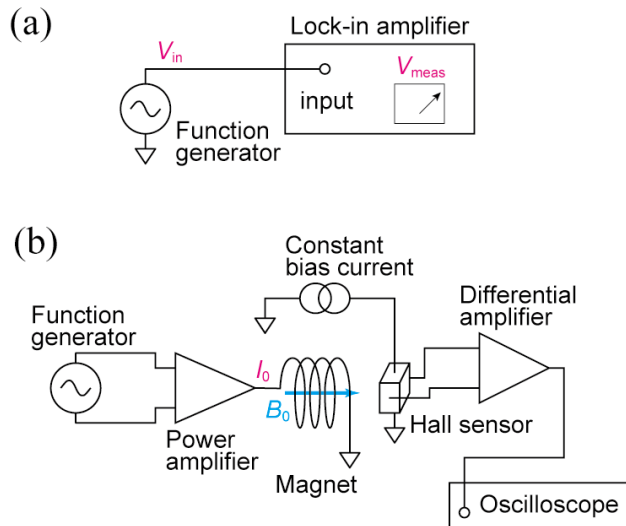


Fig. 1

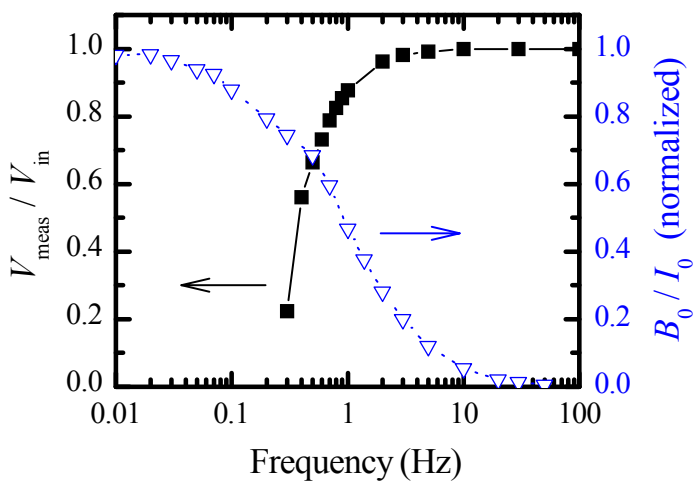


Fig. 2

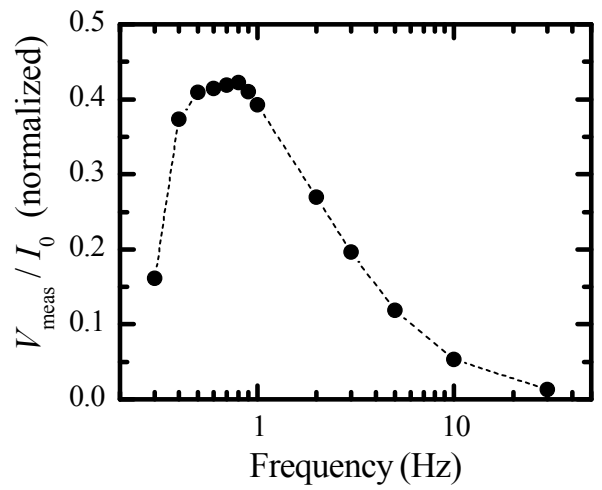


Fig. 3

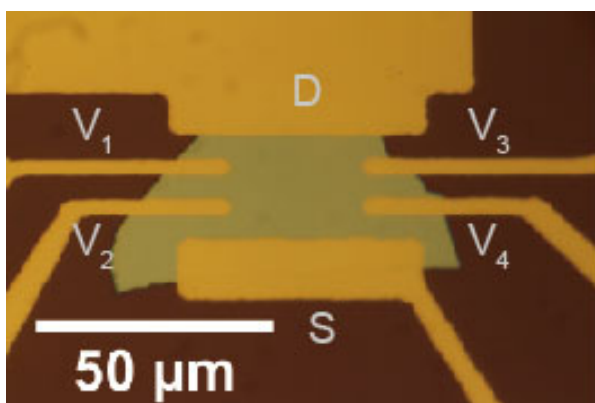


Fig. 4

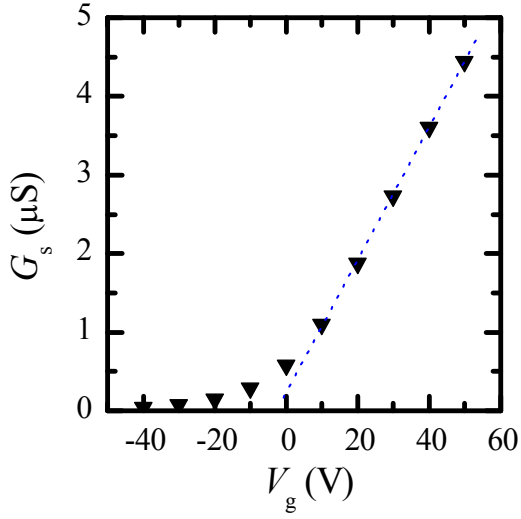


Fig. 5

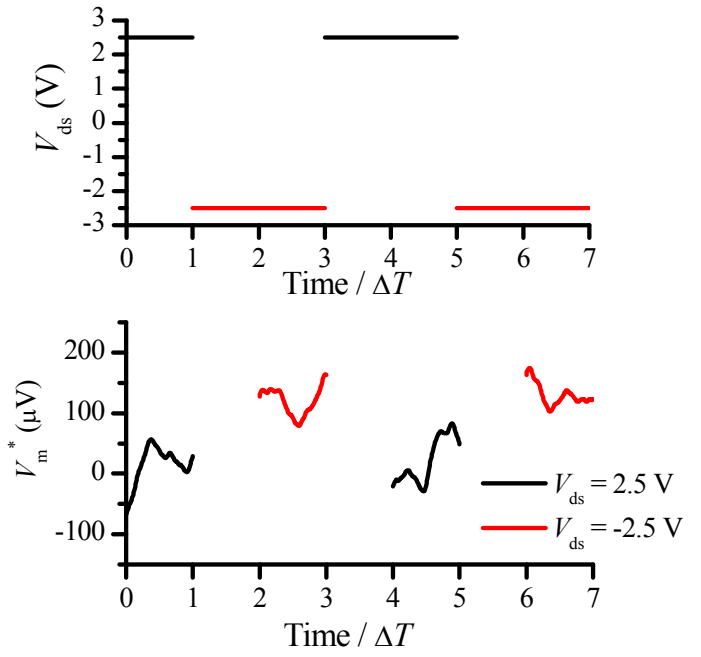


Fig. 6

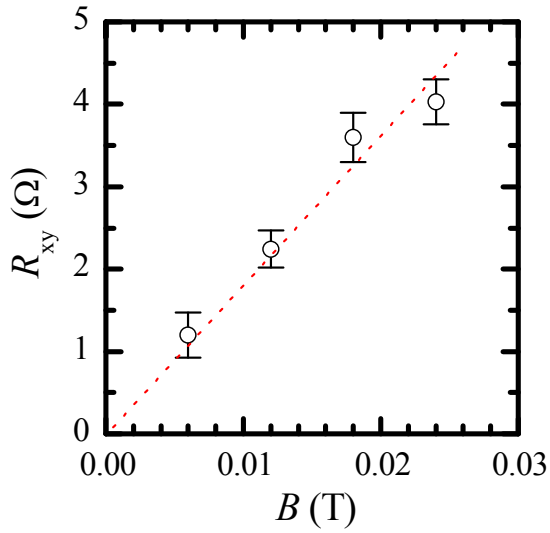


Fig. 7

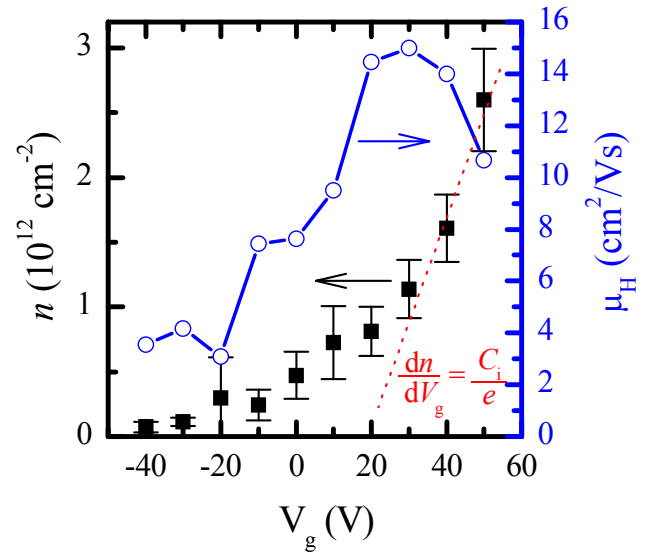


Fig. 8